Inorg. Chem. **2008**, *47*, 9509−9517

Uniform Colloidal Alkaline Earth Metal Fluoride Nanocrystals: Nonhydrolytic Synthesis and Luminescence Properties

Zewei Quan, Dongmei Yang, Piaoping Yang, Xiaoming Zhang, Hongzhou Lian, Xiaoming Liu, and Jun Lin*

State Key Laboratory of Rare Earth Resource Utilization, Changchun Institute of Applied Chemistry, Chinese Academy of Sciences, Changchun 130022, and Graduate University of the Chinese Academy of Sciences, Beijing 100049, P. R. China

Received June 11, 2008

In this paper, we present a facile and general synthetic route to high-quality alkaline earth metal fluoride (AEF_2, AE = Ca, Sr, Ba) nanocrystals and CaF_2:Tb^{3+} nanocrystals based on the thermal decomposition of corresponding trifluoroacetate precursors in hot oleylamine. X-ray diffraction, transmission electron microscopy, thermogravimetric and differential thermal analysis, Fourier transform infrared spectra, photoluminescence spectra, and kinetic decays were employed to characterize the samples. The use of single-source precursors plays an important role in the formation of high-quality AEF_2 nanocrystals, and the formation process is demonstrated in detail. The obtained AEF_2 nanocrystals are nearly monodisperse in size and highly crystalline, and they can be well dispersed in nonpolar solvents to form stable and clear colloidal solutions, which all display purple emissions under ultraviolet excitation due to the numerous surface defects of nanocrystals with large surface/volume ratios. Furthermore, we demonstrate the feasibility of introducing Tb^{3+} ions into the CaF_2 host via this method, which shows strong green emission corresponding to the characteristic $^5D_4-{}^7F_J$ ($J = 3, 4, 5, 6$) emission of Tb^{3+} ions, which can be potentially used as labels for biological molecules.

1. Introduction

The development of nanocrystals has been intensively pursued, due to increasing theoretical interest and technological demand.[1] An increasingly active part of this field is the precise control of the shape and size of dispersible colloid inorganic nanocrystals driven by their interesting size- and shape-dependent properties, as well as the assembly of advanced materials and devices by using nanoscale building blocks, and their potential applications in optics, catalysis, biosensing, and data storage.[2] Up to the present, many synthetic methods have been developed to prepare nanocrystals with a controllable shape and size, such as chemical vapor deposition, the sol−gel process, the microemulsion method, the nonhydrolytic route, and hydro-/solvothermal methods. Among them, the nonhydrolytic route, based on the thermolysis of organometallic precursors and their derivatives in exchangeable surfactant solutions, has been regarded as an efficient and robust pathway for the synthesis of high-quality nanocrystals, including metals,[3] metal oxides,[4] semiconductors,[5] and other compounds.[6] However, it is still a great challenge to identify a suitable molecular precursor and other related experimental conditions such as the

* Author to whom correspondence should be addressed. E-mail: jlin@ciac.jl.cn.

(1) (a) Iijima, S. *Nature* **1991**, *354*, 56. (b) Alivisatos, A. P. *Science* **1996**, *271*, 933. (c) Murray, C. B.; Norris, D. J.; Bawendi, M. G. *J. Am. Chem. Soc.* **1993**, *115*, 8706. (d) Lee, S. M.; Jun, Y. W.; Cho, S. N.; Cheon, J. *J. Am. Chem. Soc.* **2002**, *124*, 11244. (e) Buhro, W. E.; Colvin, V. L. *Nat. Mater.* **2003**, *2*, 138. (f) Duan, X.; Huang, Y.; Cui, Y.; Wang, J.; Lieber, C. M. *Nature* **2001**, *409*, 66. (g) Lu, W. G.; Gao, P. X.; Jian, W. B.; Wang, Z. L.; Fang, J. Y. *J. Am. Chem. Soc.* **2004**, *126*, 14816. (h) Yu, T.; Joo, J.; Park, Y. I.; Hyeon, T. *J. Am. Chem. Soc.* **2006**, *128*, 1786. (i) Wang, X.; Zhuang, J.; Peng, Q.; Li, Y. *Nature* **2005**, *437*, 121.

(2) (a) Du, Y. P.; Zhang, Y. W.; Yan, Z. G.; Sun, L. D.; Gao, S.; Yan, C. H. *Chem. Asian J.* **2007**, *2*, 965. (b) Ahmadi, T. S.; Wang, Z. L.; Green, T. C.; Henglein, A.; El-Sayed, M. A. *Science* **1996**, *272*, 1924. (c) Yin, M.; O'Brien, S. *J. Am. Chem. Soc.* **2003**, *125*, 10180. (d) Park, J.; An, K.; Hwang, Y.; Park, J. G.; Noh, H. J.; Kim, J. Y.; Park, J. H.; Hwang, N. M.; Hyeon, T. *Nat. Mater.* **2004**, *3*, 891. (e) Ahmadi, T. S.; Wang, Z. L.; Green, T. C.; Henglein, A.; El-Sayed, M. A. *Science* **1996**, *272*, 1924. (f) Bruchez, M.; Moronne, M.; Gin, P.; Weiss, S.; Alivisatos, A. P. *Science* **1998**, *281*, 2013. (g) Sun, S. H.; Murray, C. B.; Weller, D.; Folks, L.; Moser, A. *Science* **2000**, *287*, 1989.

(3) (a) Seo, W. S.; Jo, H. H.; Lee, K.; Kim, B.; Oh, S. J.; Park, J. T. *Angew. Chem., Int. Ed.* **2004**, *43*, 1115. (b) Sun, S. H.; Murray, C. B.; Weller, D.; Folks, L.; Moser, A. *Science* **2000**, *287*, 1989. (c) Puntes, V. F.; Krishnan, K. M.; Alivisatos, A. P. *Science* **2001**, *291*, 2115.

10.1021/ic8014207 CCC: $40.75
Published on Web 09/26/2008

composition of solvents and the reaction temperature and time for obtaining high-quality nanocrystals of a given inorganic material via this route.

Solid inorganic fluorides have attracted vast attention due to their uncommon properties, such as electron-acceptor behavior, high resistivity, and anionic conductivity.[7] Particularly, on the basis of their low-energy phonons and high ionicity, which lead to less absolute fundamental absorption with respect to other oxide and sulfide materials, inorganic fluorides have a wide range of potential optical applications.[8] As an important category of fluorides, alkaline earth metal fluorides (AEF_2) are dielectric and thus widely used in microelectric and optoelectric devices, such as wide-gap insulating overlayers, gate dielectrics, insulators, and buffer layers in semiconductor-on-insulator structures and more advanced 3D devices.[9] It is widely accepted that nanoscaled materials have opened the doors for finding new properties with respect to their macroscopic counterparts or enhancing the performance of currently existing devices. For example, the F^- ion conductivity can be greatly enhanced in nanophase fluorides compared with the corresponding coarse or single-crystalline phase.[10] Therefore, the synthesis of AEF_2 nanocrystals has aroused much interest, and many methods including microemulsion,[11a−c] hydrothermal treatment,[11d] and the polyol route[11e] have been explored to prepare AEF_2 nanocrystals. However, up to now, there have been few reports on the general synthesis of AEF_2 nanocrystals with uniform shape and good solubility in organic solvents (high-quality colloid nanocrystals). The main reason rests with the rapid precipitation reaction between alkaline earth metal salts and NaF/NH_4F in aqueous or polyol solutions that have been generally adopted in previous studies. Therefore, the first step in achieving high-quality colloidal nanocrystals is the selection of a suitable molecular precursor for AEF_2. According to Rüssel et al.,[12,13] it is known that metal trifluoroacetates can thermally decompose at elevated temperatures to give the corresponding metal fluorides and various fluorinated and oxyfluorinated carbon species. Furthermore, both metal and fluorine elements are integrated in the same compound, which may provide a much better controlled-synthesis of fluoride nanocrystals than the liquid precipitation methods. Therefore, in our work, we adopt alkaline earth metal trifluoroacetates as single-source precursors (SSPs) to achieve the controlled nucleation and growth of AEF_2 nanocrystals that is a prerequisite to obtaining monodisperse nanocrystals. Furthermore, the use of a coordinating solvent that can efficiently confine the particle growth and provide good solubility in nonpolar solution for the synthesis of various types of nanocrystals is also well documented.[14] Therefore, we develop a novel route that exploits the combination of these two facts to prepare high-quality colloidal AEF_2 nanocrystals. On the other hand, fluoride nanoparticles doped with lanthanide(III) ions have been reported to display unique luminescence properties arising from their 4f electron configuration.[15] Specially, the lanthanide(III) ions incorporated in the CaF_2 will cause an increase in the refractive index with respect to the pure CaF_2, which makes it very attractive as an active waveguide to realize optical integrated devices.[16]

In this paper, we present a simple one-pot route for the general synthesis of high-quality colloidal AEF_2 (AE = Ca, Sr, Ba) nanocrystals and Tb^{3+}-doped CaF_2 nanocrystals via the thermal decomposition of corresponding metal trifluoroacetates in the coordinating solvent oleylamine (OM). These obtained AEF_2 nanocrystal colloidal solutions all present a purple emission under ultraviolet excitation, due to the numerous surface defects that are caused by the large surface/volume ratio of nanocrystals. Furthermore, this purple emission can be adjusted to a green color after the successful incorporation of Tb^{3+} ions into CaF_2 nanocrystals.

2. Experimental Section

Materials. Alkaline earth metal carbonates ($CaCO_3$, $SrCO_3$, and $BaCO_3$), Tb_4O_7, trifluoroacetic acid (CF_3COOH), absolute ethanol, and cyclohexane were all analytical-grade and purchased from Beijing Beihua Chemicals Co., Ltd. OM (70%, technical grade)

(4) (a) Si, R.; Zhang, Y. W.; You, L. P.; Yan, C. H. *Angew. Chem., Int. Ed.* **2005**, *44*, 3256. (b) Si, R.; Zhang, Y. W.; Zhou, H. P.; Sun, L. D.; Yan, C. H. *Chem. Mater.* **2007**, *19*, 18. (c) Cheon, J.; Kang, N.-J.; Lee, S. M.; Lee, J. H.; Yoon, J. H.; Oh, S. J. *J. Am. Chem. Soc.* **2004**, *126*, 1950.

(5) (a) Trindade, T.; O'Brien, P.; Zhang, X.-M. *Chem. Mater.* **1997**, *9*, 523. (b) Peng, X.; Manna, L.; Yang, W.; Wickham, J.; Scher, E.; Kadavanich, A.; Alivisatos, A. P. *Nature* **2000**, *404*, 59. (c) Monge, M.; Kahn, M. L.; Maisonnat, A.; Chaudret, B. *Angew. Chem., Int. Ed.* **2003**, *42*, 5321.

(6) (a) Kömpe, K.; Borchert, H.; Storz, J.; Lobo, A.; Adam, S.; Möller, T.; Haase, M. *Angew. Chem., Int. Ed.* **2003**, *42*, 5513. (b) Stouwdam, J. W.; van Veggel, F. C. J. M. *Nano Lett.* **2002**, *2*, 733.

(7) Peng, G.; Xie, Y.; Li, Z. *Eur. J. Inorg. Chem.* **2006**, *16*, 3261.

(8) Justel, T.; Nikol, H.; Ronda, C. *Angew. Chem., Int. Ed.* **1998**, *37*, 3085.

(9) Singh, R.; Sinha, S.; Chou, P.; Hsu, N. J.; Radpour, F. *J. Appl. Phys.* **1989**, *66*, 6179.

(10) Sata, N.; Eberman, K.; Eberl, K.; Maier, J. *Nature* **2000**, *408*, 946.

(11) (a) Cao, M. H.; Hu, C. W.; Wang, E. B. *J. Am. Chem. Soc.* **2003**, *125*, 11196. (b) De, G. J. H.; Qin, W. P.; Zhang, J. S.; Zhang, J. S.; Wang, Y.; Cao, C. Y.; Cui, Y. *J. Solid State Chem.* **2006**, *179*, 955. (c) Lian, H. Z.; Ye, Z. R.; Shi, C. S. *Nanotechnology* **2004**, *15*, 1455. (d) Sun, X. M.; Li, Y. D. *Chem. Commun.* **2003**, 1768. (e) Feldmann, C.; Roming, M.; Trampert, K. *Small* **2006**, *2*, 1248. (f) Grass, R. N.; Stark, W. J. *Chem. Commun.* **2005**, 1767. (g) Gao, P.; Xie, Y.; Li, Z. *Eur. J. Inorg. Chem.* **2006**, *16*, 3261.

(12) (a) Rüssel, C. *J. Non-Cryst. Solids* **1993**, *152*, 161. (b) Rillings, K. W.; Roberts, J. E. *Thermochim. Acta* **1974**, *10*, 285.

(13) (a) Zhang, Y. W.; Sun, X.; Si, R.; You, L. P.; Yan, C. H. *J. Am. Chem. Soc.* **2005**, *127*, 3260. (b) Mai, H. X.; Zhang, Y. W.; Si, R.; Yan, Z. G.; Sun, L. D.; You, L. P.; Yan, C. H. *J. Am. Chem. Soc.* **2006**, *128*, 6426. (c) Sun, X.; Zhang, Y. W.; Du, Y. P.; Yan, Z. G.; Si, R.; You, L. P.; Yan, C. H. *Chem.—Eur. J.* **2007**, *13*, 2320.

(14) (a) Lu, W. G.; Ding, Y.; Chen, Y. X.; Wang, Z. L.; Fang, J. Y. *J. Am. Chem. Soc.* **2005**, *127*, 10112. (b) Lu, W. G.; Fang, J. Y.; Stokes, K. L.; Lin, J. *J. Am. Chem. Soc.* **2004**, *126*, 11798.

(15) (a) Stouwdam, J. W.; van Veggel, F. C. J. M. *Nano Lett.* **2002**, *2*, 733. (b) Bender, C. M.; Burlitch, J. M. *Chem. Mater.* **2000**, *12*, 1969. (c) Wojtowicz, A. J. *Nucl. Instrum. Methods A* **2002**, *486*, 201. (d) Wang, F.; Fan, X. P.; Pi, D. B.; Wang, M. Q. *Solid State Commun.* **2005**, *133*, 775.

(16) Balaji, T.; Lifante, G.; Daran, E.; Legros, R.; Lacoste, G. *Thin Solid Films* **1999**, *339*, 187.

(17) (a) Roberts, J. E. *J. Am. Chem. Soc.* **1961**, *83*, 1087. (b) Xia, Y.; Whiteside, G. M. *Annu. Rev. Mater. Sci.* **1998**, *28*, 153. (c) Hu, J.; Beck, R. G.; Whiteside, R. M. *Adv. Mater.* **1998**, *10*, 574. (d) Seraji, S.; Wu, Y.; Jewell-Larson, N. E.; Forbess, M. J.; Limmer, S. J.; Chou, T. P.; Cao, G. *Adv. Mater.* **2000**, *12*, 1421. (e) Yu, M; Lin, J.; Wang, Z.; Fu, J.; Wang, S.; Zhang, H. J.; Han, Y. C. *Chem. Mater.* **2002**, *14*, 2224.

(18) (a) Kingery, W. D.; Bowen, H. K.; Uhlmann, D. R. *Introduction to Ceramics*; Wiley: New York, 1976. (b) Shannon, R. D. *Acta Crystallogr.* **1976**, *A32*, 751.

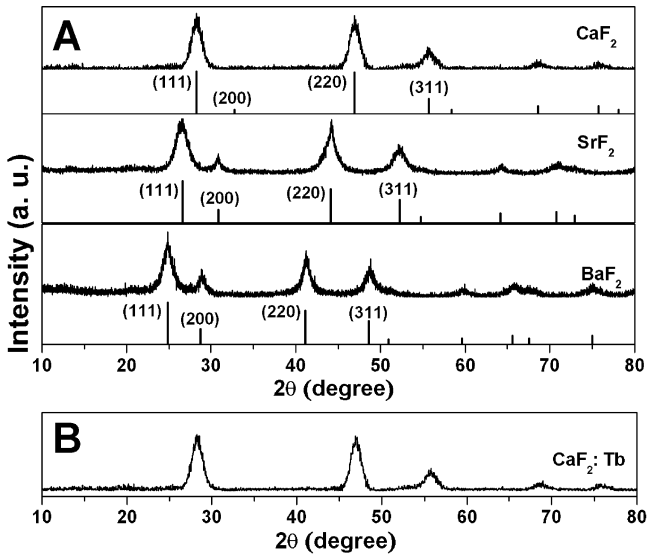

Figure 1. XRD patterns of CaF_2, SrF_2, and BaF_2 nanocrystals (A) and CaF_2:0.05Tb^{3+} nanocrystals (B).

was purchased from Aldrich. All of the materials were used without further purification.

Preparation of Trifluoroacetate Precursors. Trifluoroacetate precursors were prepared from the corresponding carbonates or oxides according to the literature method.[17a] In a typical synthesis, alkaline earth metal carbonate or Tb_4O_7 was added in slight excess to trifluoroacetic acid with the evolution of heat and continuous stirring to make the reaction occur rapidly. Then, the mixture was allowed to stand overnight, and the excess carbonate or Tb_4O_7 was filtered. The transparent trifluoroacetate solution was dried in an oven at 100 °C for 12 h to obtain trifluoroacetate powders.

Synthesis of AEF_2 (AE = Ca, Sr, Ba) Nanocrystals. In a typical synthesis, 1 mmol of alkaline earth metal trifluoroacetate was then added to the three-neck round-bottom reaction vessel with 10 mL of OM, and then the mixture was heated to 100 °C under a vacuum with magnetic stirring for 30 min to remove residual water and oxygen. At this stage, a colorless transparent solution was formed, and subsequently, this solution was rapidly heated to 280 °C under an argon atmosphere and maintained for 1 h. When the reaction was completed, this solution was allowed to cool to room temperature. Subsequently, the nanocrystals were precipitated by the addition of excess ethanol, isolated via centrifugation, washed three times with ethanol, and finally dried in oven at 80 °C for 1 h. The finally obtained nanocrystals could be readily dispersed in nonpolar solvents such as cyclohexane, toluene, and chloroform to form a colorless transparent colloid solution.

Synthesis of CaF_2:Tb^{3+} Nanocrystals. The synthesis procedure was basically identical to that for the synthesis of AEF_2 nanocrystals, except that 0.05 mmol of terbium trifluoroacetate was added into the reaction vessel together with 1 mmol of calcium trifluoroacetate at the first step.

Characterization. Powder X-ray diffraction (XRD) measurements were performed on a Rigaku-Dmax 2500 diffractometer with graphite monochromatized Cu Kα radiation (λ = 0.15405 nm). Thermogravimetric and differential thermal analysis (TG-DTA) data were recorded with a Thermal Analysis Instrument (SDT 2960, TA Instruments, New Castle, DE) with a heating rate of 10 °C/min in an air flow of 100 mL/min. Fourier transform infrared (FT-IR) spectra were measured with a Perkin-Elmer 580B infrared spectrophotometer with the KBr pellet technique. Transmission electron microscopy (TEM) was performed using a FEI Tecnai G2 S-Twin with a field emission gun operating at 200 kV, and images were acquired digitally on a Gatan multipole CCD camera. Samples for TEM were prepared by depositing a drop of sample dispersed in cyclohexane onto a carbon grid. The excess liquid was wicked away with filter paper, and the grid was dried at 70 °C for 1 h in a vacuum-dryer. The excitation and emission photoluminescence (PL) spectra were taken on an F-4500 spectrophotometer equipped with a 150 W xenon lamp as the excitation source. The luminescence decay curves were obtained from a Lecroy Wave Runner 6100 Digital Osilloscope (1 GHz) using a tunable laser (pulse width = 4 ns, gate = 50 ns) as the excitation (Contimuum Sunlite OPO). The spectra and decay curves were both obtained from samples dispersed in cyclohexane solutions. All of the measurements were performed at room temperature.

3. Results and Discussion

3.1. Structure, Morphology, and Formation of AEF_2 (AE= Ca, Sr, Ba) and CaF_2: Tb^{3+} Nanocrystals. Structure. Figure 1A shows the XRD patterns of the as-prepared CaF_2, SrF_2, and BaF_2 nancocrystals, and vertical bars below each pattern are their corresponding standard cards (JCPDS Card No. 65-0535 (CaF_2), 06-0262 (SrF_2), and 04-0452 (BaF_2), respectively). It is obvious that all of the XRD patterns of these three samples can be indexed to a pure face-centered cubic phase (*fcc*, space group: *Fm*3*m*), and these are consistent with the values in the standard cards. The calculated cell parameters (a) of the as-prepared CaF_2, SrF_2, and BaF_2 nanocrystals are 0.547, 0.579, and 0.620 nm, respectively, and are close to those of the corresponding bulk CaF_2 (0.547 nm), SrF_2 (0.580 nm), and BaF_2 (0.620 nm) crystals, respectively. It can be seen that the main diffraction peaks such as the (111), (220), and (311) planes in the XRD patterns of these three samples are obviously broadened, attributable to the small-size nature of nanocrystals, and they can be used to estimate the average crystallite size by Scherer's formula. ($D_{hkl} = K\lambda/(\beta \cos \theta)$, where λ is the X-ray wavelength (0.15405 nm), β is the full width at half-maximum, θ is the diffraction angle, K is a constant (0.89), and D_{hkl} means the size along the (hkl) direction). The estimated average crystallite sizes are 6.2 nm (CaF_2), 8.3 nm (SrF_2), and 11.6 nm (BaF_2), respectively, which agree well with those observed from TEM images in the next part.

Figure 1B shows the XRD pattern of CaF_2:0.05Tb^{3+} nanocrystals. All of the detectable peaks can be indexed to almost the same positions as those from the standard bulk CaF_2 crystals and from the obtained pure CaF_2 nanocrystals (Figure 1A); however, a slight increase of the lattice constant for CaF_2:0.05Tb^{3+} nanocrystals (0.549 nm) is observed, compared to 0.547 nm for pure CaF_2 nanocrystals. However, according to Vegard's law,[18a] the cubic lattice parameter of Tb^{3+}-ion-doped CaF_2 crystals will shrink slightly in comparison with that of pure CaF_2 crystals, since the eight-coordinate Tb^{3+} ion has a smaller radius than the eight-coordinate Ca^{2+} ion (0.104 nm for Tb^{3+} ion vs 0.112 nm for Ca^{2+} ion).[18b] The exceptional increase of lattice parameters may be ascribed to the formation of the interstitial fluorine ions. In rare-earth-ion-doped alkaline earth fluoride, as had been well established, rare earth ions will enter the alkaline earth fluoride lattice to substitute alkaline earth ions and may reside in a variety of sites. The rare earth ions whose

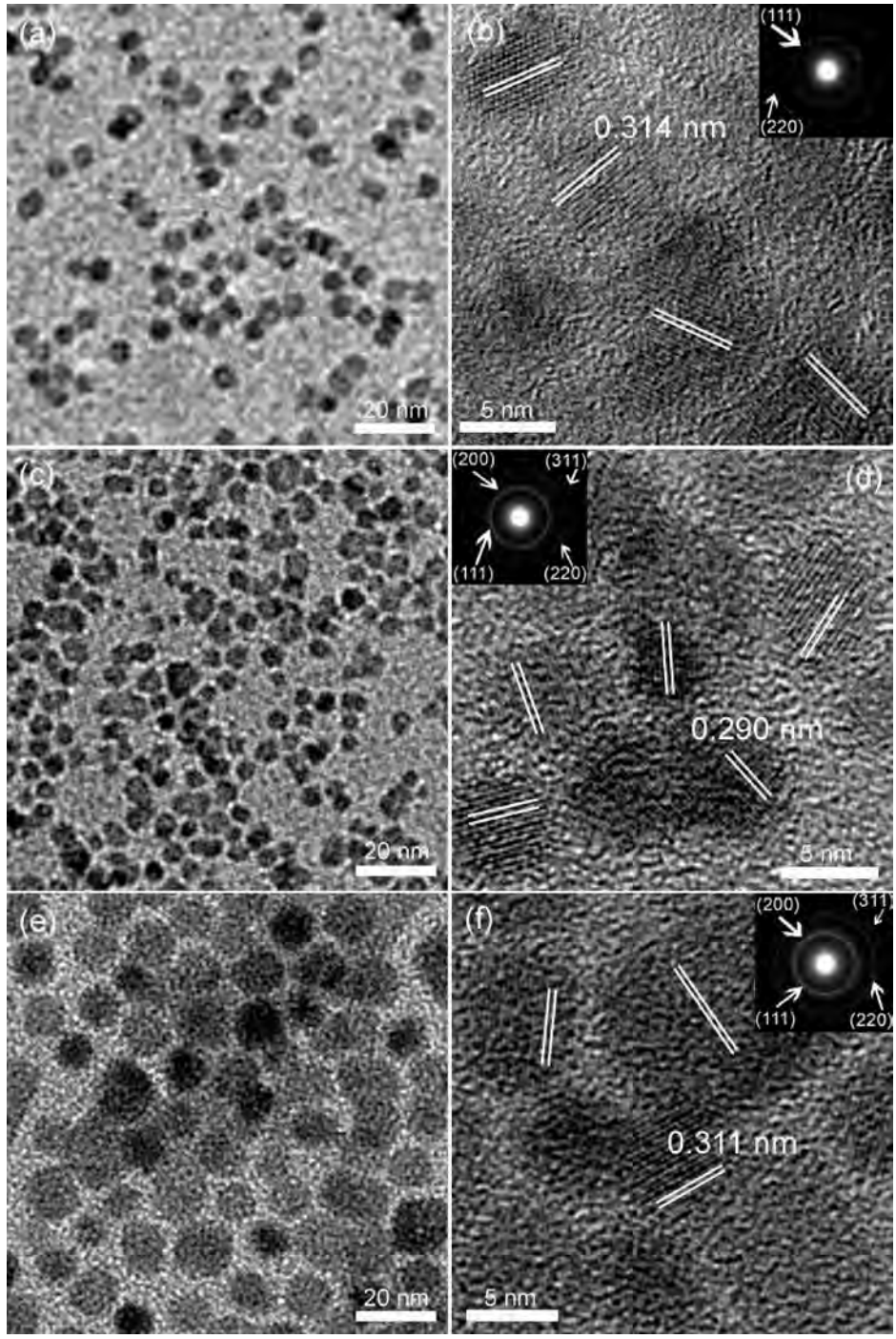

Figure 2. TEM and HRTEM images of CaF_2 (a and b), SrF_2 (c and d), and BaF_2 (e and f) nanocrystals. Insets of b, d, and f are their corresponding selected area electron diffraction (SAED) patterns.

charges are not locally compensated will form centers of cubic (O_h) symmetry. Alternatively, the charges may be compensated by the formation of interstitial fluorine ions in either nearest-neighbor or next-nearest-neighbor positions, forming tetragonal (C_{4v}) or trigonal (C_{3v}) centers, respectively.[19] It is the presence of interstitial fluorine ions that enlarges the crystal lattice, leading to an increase of the lattice parameter for CaF_2:0.05Tb^{3+} nanocrystals. Therefore, the change in lattice parameter can to some extent prove the successful doping of Tb^{3+} ions into the host lattice of CaF_2 nanocrystals rather than adhering as absorbed species, since no change in lattice parameters could be observed if Tb^{3+} ions did not substitute for the Ca^{2+} ions.

Morphology. Figure 2 displays the TEM and HRTEM images of AEF_2 nanocrystals, demonstrating that all of the as-obtained AEF_2 nanocrystals are relatively uniform in size and morphology and of a single-crystalline nature. Panels a,

(19) (a) Catlow, C. R. A. *J. Phys. C* **1976**, *9*, 1845. (b) Catlow, C. R. A. *J. Phys. C* **1976**, *9*, 1859. (c) Wckoever, S. W. S.; Brown, M. D.; Abbundi, T. J.; Chan, H.; Mathur, V. K. *J. Appl. Phys.* **1986**, *60*, 2505. (d) Cirillo-Penn, K. M.; Wright, J. C. *J. Lumin.* **1991**, *48*−*49*, 505.
(20) (a) Wang, Z. L. *J. Phys. Chem. B* **2000**, *104*, 1153. (b) Xiong, Y.; Xia, Y. *Adv. Mater.* **2003**, *19*, 3385.

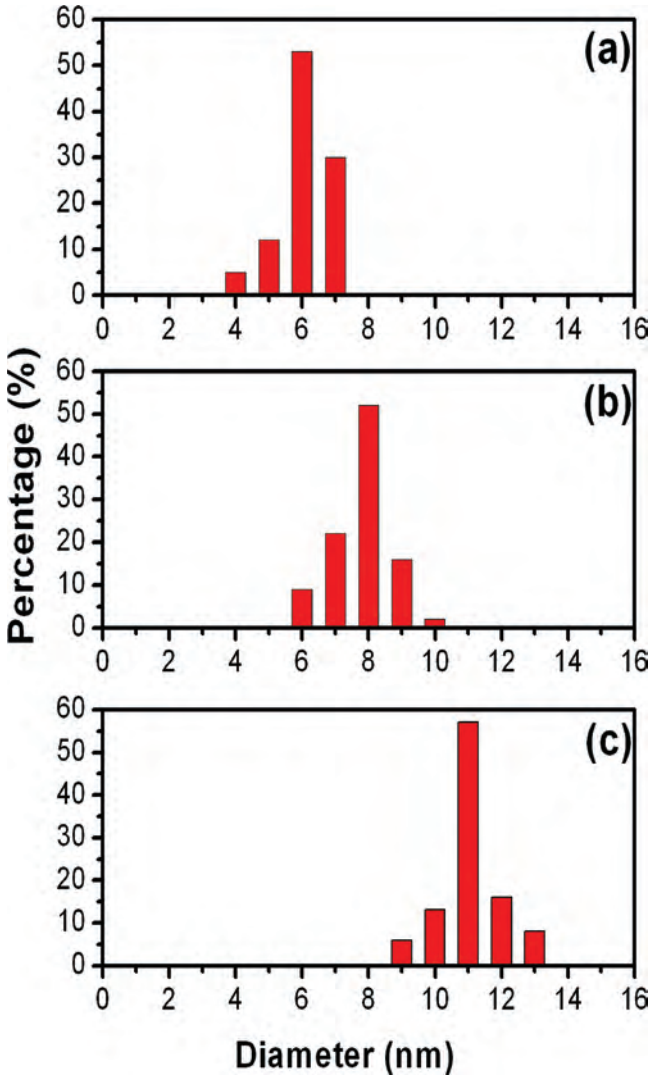

Figure 3. Particle size distribution histograms of the CaF_2 (a), SrF_2 (b), and BaF_2 (c) nanocrystals counted from the TEM images.

c, and e of Figure 2 show the TEM images of CaF_2, SrF_2, and BaF_2 nanocrystals without any further size-selection process, respectively. All of the samples seem to be near-spherical shape and have average size of 6.5 nm for CaF_2, 8.5 nm for SrF_2, and 11.2 nm for BaF_2, respectively. Figure 3 shows the particle size distribution histograms of the CaF_2 (a), SrF_2 (b), and BaF_2 (c) nanocrystals counted from the TEM images, clearly demonstrating their relatively uniform morphologies. The HRTEM images of CaF_2 (b), SrF_2 (d), and BaF_2 (f) nanocrystals reveal the fringes from the continuous lattice structure of a typical crystallite, indicating that these nanocrystals are of single-crystalline nature. The insets of b, d, and f are their corresponding selected area electron diffraction (SAED) patterns, in which all of the diffraction rings can be ascribed to specific crystal planes of their corresponding XRD patterns shown in Figure 1A. It should be noted that the presence of ring-shaped SAED patterns is not in conflict with their single-crystalline nature, because the SAED patterns were recorded from an area containing a large number of nanocrystals. As for CaF_2 nanocrystals shown in Figure 2b, the distance (0.314 nm) between the adjacent lattice fringes agrees well with the (111)

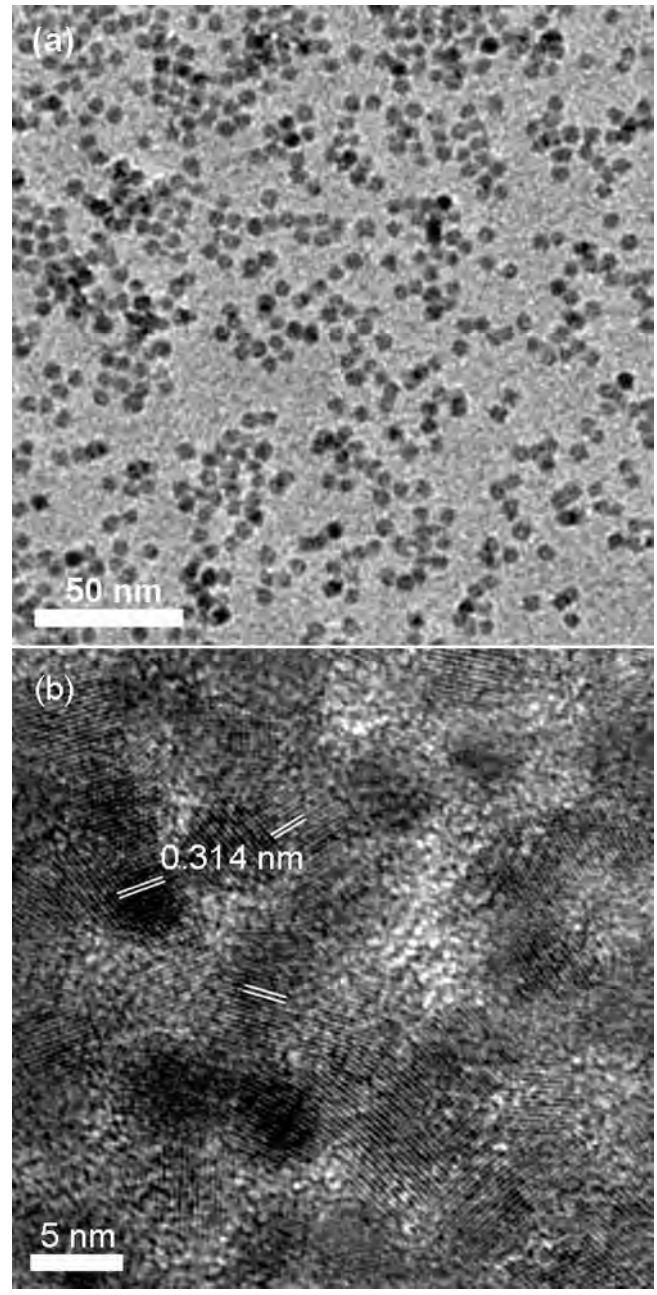

Figure 4. TEM (a) and HRTEM (b) images of CaF_2:0.05Tb^{3+} nanocrystals.

d spacing of bulk CaF_2 (0.316 nm). While, as for the SrF_2 and BaF_2 nanocrystals shown in Figure 2d and f, the adjacent fringe distances, 0.290 nm for SrF_2 and 0.311 nm for BaF_2, are basically consistent with the (200) *d* spacings of bulk SrF_2 (0.290 nm) and BaF_2 (0.310 nm), respectively.

After the incorporation of the Tb^{3+} ion into a CaF_2 host, the obtained corresponding TEM and HRTEM images (Figure 4) indicate that as-synthesized doped nanocrystals possess almost identical shape and size to that of pure CaF_2 nanocrystals, and the distances between the adjacent lattice fringes, measured as 0.318 nm, agree well with the literature value for the (111) *d* spacing of bulk CaF_2, 0.316 nm. Furthermore, no lattice fringes ascribed to other phases such as TbF_3 are observed in this HRTEM image. These results

further confirm that the Tb^{3+} ions have been successfully built into the CaF_2host lattices.

Surface Structure. It is well-known that the formation of a stable colloidal solution can be attributed to the equilibrium built between the van der Waals attractive forces and the steric repulsions from the capping ligand.[22] It is the OM ligand in our system that provides the obtained AEF_2 nanocrystals with excellent stability and solubility in cyclohexane solutions, as shown in Figure 5a and c. It should be noted that a further Tyndall effect study (Figure 5b), in which light scattering is obviously observed for these three cyclohexane solutions of AEF_2 nanocrystals, can be used to confirm their colloidal nature. The presence of the OM ligand can be proved from the representative FT-IR spectrum of CaF_2 nanocrystals, as shown in the bottom part of Figure 6. It shows a broad absorption peak at 3431 cm^{-1} that can be ascribed to the asymmetric stretching vibration of the primary amino (NH_2) group.[23] In addition, the presence of the absorption peak at 1583 cm^{-1}, which is regarded as the only definitive and valuable peak of the NH_2 group in the case of scissoring vibration, can further confirm the existence of a NH_2 group in the obtained CaF_2 nanocrystals.[21a] The peaks at 1678 cm^{-1} and 3006 cm^{-1} are assigned to the stretching vibration of C═C and ═C−H, respectively, implying the presence of a CH═CH group in the final products.[24] The 2957 cm^{-1} shoulder on the peak at 2925 cm^{-1} and the peak at 1462 cm^{-1} are the antisymmetric stretching vibration and asymmetrical deformation frequency of methyl.[21a] The sharp peaks at 2853 and 2925 cm^{-1} are assigned to the symmetric and antisymmetric stretching vibration of the $-CH_2$ group, and the peak at 721 cm^{-1} is assigned to the in-planar swing of $(CH_2)_n$ ($n > 4$).[24] Through the above analysis, we can conclude that the as-prepared CaF_2 nanocrystals have been capped by OM molecules successfully, and the same situation holds for the as-prepared SrF_2 and BaF_2 nanocrystals.

Formation Process. In this system, the single-source precursors of alkaline earth metal trifluoroacetates are adopted and play an important role in the formation of high-quality AEF_2 nanocrystals. A series of measurements were thus conducted to investigate the as-formed alkaline earth metal trifluoroacetate precursors that are denoted as p-CaF_2, p-SrF_2, and p-BaF_2, respectively. According to their XRD results, as shown in Figure S1 (Supporting Information), there are no standard diffraction patterns in the JCPDS reference database that match well the obtained XRD patterns. Therefore, further TG-DTA measurements of the precursors (p-CaF_2, p-SrF_2, and p-BaF_2) were conducted to obtain the detailed thermolysis information of these precursors, as shown in Figure S2 (Supporting Information). The TG curve of p-CaF_2 shows two stages of weight loss. The first weight loss step (5%) is observed between 60 and 100 °C due to the evaporation of absorbed water accompanied by an endothermic peak at 94 °C. The second weight loss (70.5%) is in the range of 278−350 °C, accompanied by a strong exothermic peak at 344 °C in the DTA curve due to the rapid decomposition of p-CaF_2 into CaF_2, which is confirmed by the above XRD results of finally obtained nanocrystals. Therefore, the molecular weight of p-CaF_2 is estimated to be 264, and therefore the corresponding molecular weight of the anion group is finally about 112, agreeing well with

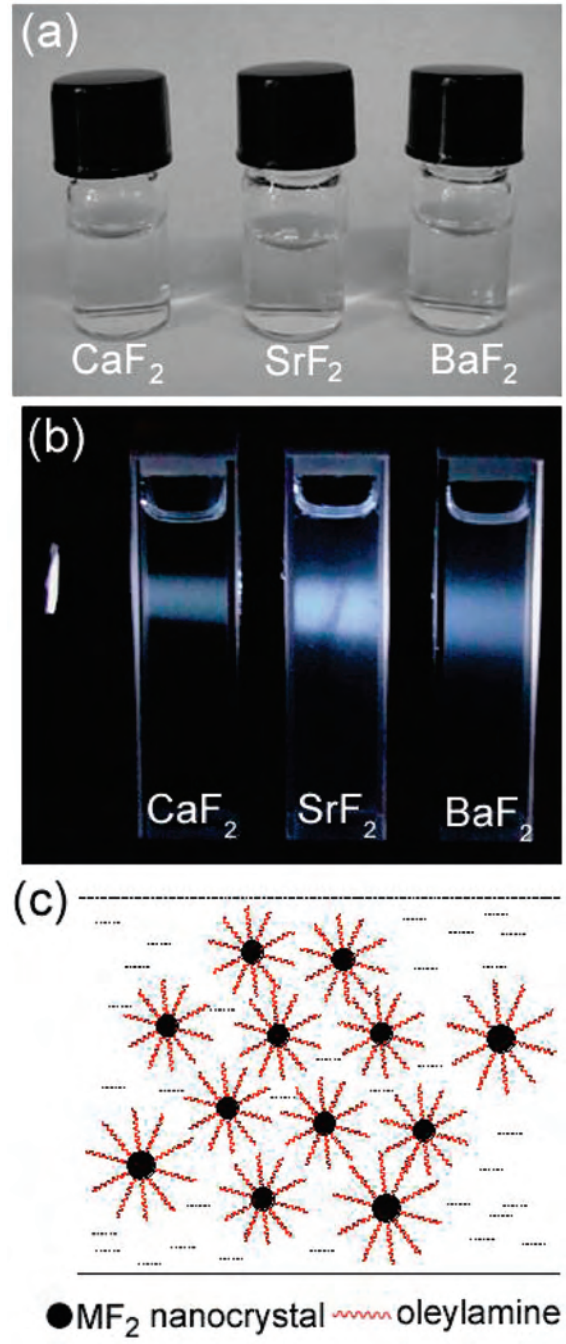

Figure 5. Digital images of cyclohexane solutions of CaF_2, SrF_2, and BaF_2 nanocrystals under daylight (a) and under flashlight irradiation in the dark (b), as well as the model (c) illustrating the structure of obtained nanocrystals in cyclohexane solution.

(21) (a) Park, J.; Kang, E.; Son, S. U.; Park, H. M.; Lee, M. K.; Kim, J.; Kim, K. W.; Noh, H. J.; Park, J. H.; Bae, C. J.; Park, J. G.; Hyeon, T. *Adv. Mater.* **2005**, *17*, 429. (b) Dean, J. A. *Lange's Handbook of Chemistry*, 15th ed.; McGraw-Hill: New York, 1999.
(22) (a) Li, Y. C.; Li, X. H.; Yang, C. H.; Li, Y. F. *J. Phys. Chem. B* **2004**, *108*, 16002. (b) Quan, Z. W.; Wang, Z. L.; Yang, P. P.; Lin, J.; Fang, J. Y. *Inorg. Chem.* **2007**, *46*, 1354.
(23) (a) Rao, C. N. R. *Chemical Applications of Infrared Spectroscopy*; Academic: New York, 1963. (b) Kong, D. Y.; Wang, Z. L.; Lin, C. K.; Quan, Z. W.; Li, C. X.; Lin, J. *Nanotechnology* **2007**, *18*, 075601.
(24) Zhang, X. M.; Quan, Z. W.; Yang, J.; Yang, P. P.; Lian, H. Z.; Lin, J. *Nanotechnology* **2008**, *19*, 075603.

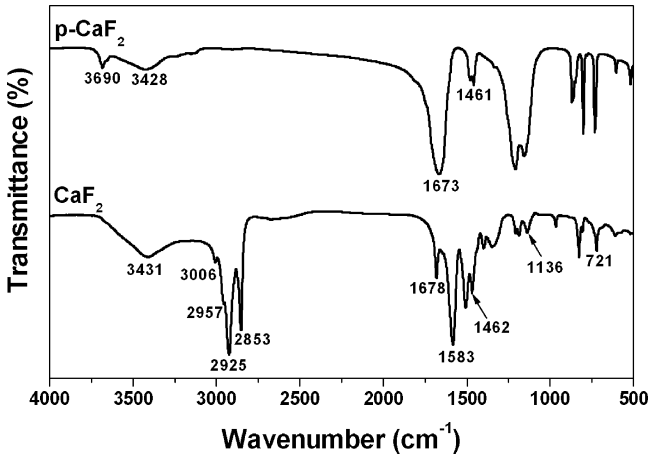

Figure 6. FT-IR spectra of *p*-CaF_2 and CaF_2 nanocrystals.

the molecular weight of CF_3COO^-. This point can be further confirmed by the presence of the stretching vibrations of carboxylate COO^- (1461 and 1673 cm^{-1}) in the FT-IR spectrum of p-CaF_2,[24] as shown in the top part of Figure 6. In addition, the broad absorption band peaking at 3690 and 3428 cm^{-1} is due to the stretching vibration of the hydroxyl group (−OH) of absorbed water molecules.[23a] Therefore, the molecular formula of p-CaF_2 should be $Ca(CF_3COO)_2 \cdot H_2O$. Similar situations can also be observed for p-SrF_2 and p-BaF_2, and their final molecular formulas are determined as $Sr(CF_3COO)_2 \cdot H_2O$ and $Ba(CF_3COO)_2 \cdot H_2O$, respectively. On the basis of the above results, the compositions of these SSPs are determined, indicating the successful preparation of alkaline earth metal trifluoroacetate precursors.

It is well-known that the key to the synthesis of high-quality nanocrystals is the burst of nucleation, also referred to as the separation of nucleation and growth.[25] Up to now, there have been two techniques that utilize homogeneous nucleation to synthesize monodisperse nanocrystals in the organic solutions: "hot-injection" and "heating-up" methods.[26] The former technique produces high supersaturation, which is induced by rapid injection of the highly reactive reactants into a hot surfactant solution. It leads to the fast homogeneous nucleation reaction, which is followed by the diffusion-controlled growth process, in which "focusing" of the particle size distribution occurs.[26a,27] It has been widely used to synthesize nanocrystals of metal chalcogenides and nitrides[28] and transition and noble metals.[29] On the other hand, the heating-up technique is a one-pot process in which the precursors, reagents, and solvent are mixed at a low temperature and heated up to a certain temperature to initiate the crystallization reaction.[25b] Recent studies on the mechanism of this growth process indicate that a sudden increase in the number concentration of the nanocrystals (burst of nucleation) is followed by a rapid narrowing of the size distribution (size focusing).[23a] This technique can produce uniform nanocrystals with a size distribution comparable to that obtained using the "hot-injection" method. The heating-up method is particularly advantageous for large-scale production, because of its simplicity compared with the hot-injection method.

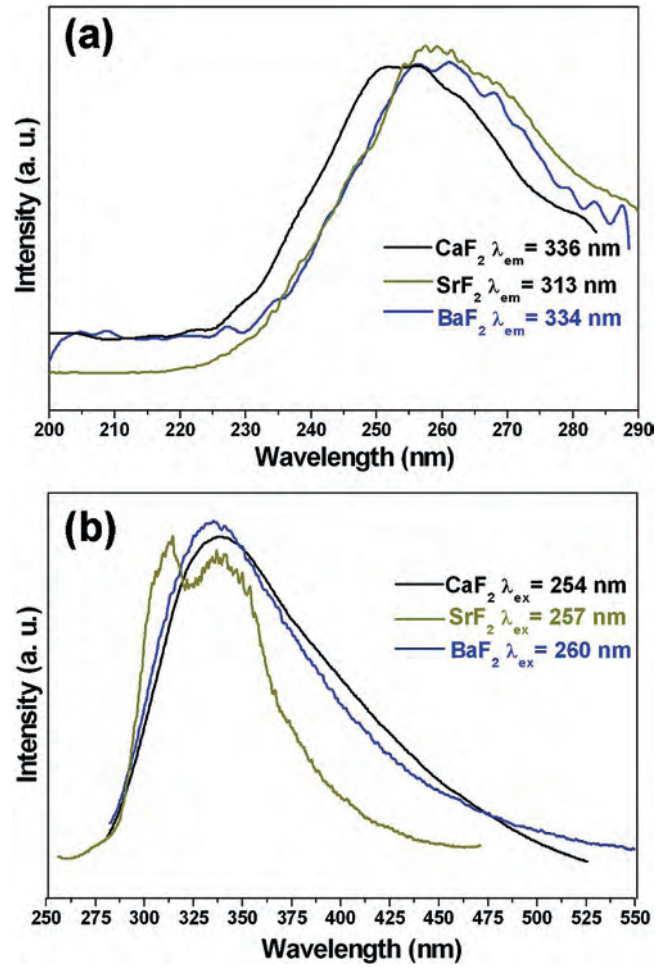

Figure 7. PL excitation and emission spectra of CaF_2:$0.05Tb^{3+}$ nanocrystals dispersed in cyclohexane solutions. The inset is the digital image of a CaF_2:$0.05Tb^{3+}$ colloidal solution under 254 nm UV lamp irradiation.

In our system, high-quality AEF_2 nanocrystals have been successfully prepared via the heating-up method, in which the corresponding alkaline earth metal trifluoroacetates and OM are adopted as precursors and the solvent, respectively. As the transparent reaction mixture reached the thermolysis temperature of alkaline earth metal trifluoroacetates, some tiny gas bubbles were emitted promptly from the reaction system, which implied an instant decomposition of the precursor and a simultaneous formation of homogeneous nuclei. According to the thermolysis reaction of trifluoroacetate shown below, the gas bubbles were determined as CO_2 and fluorinated carbon species.[12a]

$$AE(CF_3COO)_2 \rightarrow AEF_2 + C_2F_4 + 2CO_2 \qquad (1)$$

As for the structure of alkaline earth metal trifluoroacetates, alkaline earth metal ions were coordinated by oxygen atoms; therefore, it is rational that the retention of the AE−O bond

(25) (a) Sugimoto, T. *Monodispersed Particles*; Elsevier: Amsterdam, 2001. (b) Sugimoto, T. *Adv. Colloid Interface Sci.* **1987**, *28*, 65. (c) LaMer, V. K.; Dinegar, R. H. *J. Am. Chem. Soc.* **1950**, *72*, 4847. (d) Peng, Z. A.; Peng, X. *J. Am. Chem. Soc.* **2002**, *124*, 3343.

(26) (a) Kwon, S. G.; Piao, Y.; Park, J.; Angappane, S.; Jo, Y.; Hwang, N. M.; Park, J. G.; Hyeon, T. *J. Am. Chem. Soc.* **2007**, *129*, 12571. (b) Park, J.; Joo, J.; Kwon, S. G.; Jang, Y.; Hyeon, T. *Angew. Chem., Int. Ed.* **2007**, *46*, 4630.

(27) Murray, C. B.; Norris, D. J.; Bawendi, M. G. *J. Am. Chem. Soc.* **1993**, *115*, 8706.

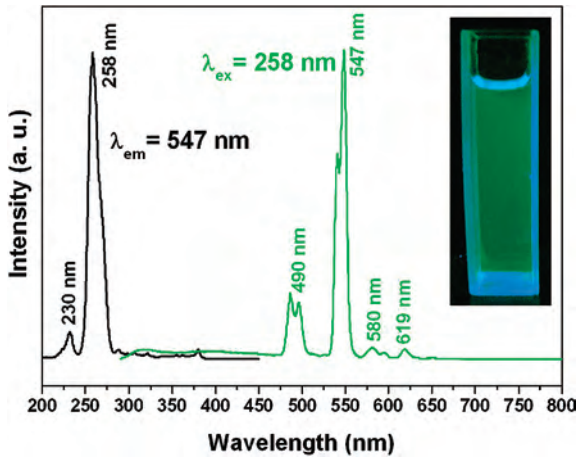

Figure 8. PL excitation (a) and emission (b) spectra of CaF_2, SrF_2, and BaF_2 nanocrystals dispersed in cyclohexane solutions.

would occur in the initial nucleation stage.[2a] At the same time, F^- ions were produced due to cleavage of the C−F bonds of the CF_3COO^- ligands in solution. Promptly, solid AEF_2 nuclei were generated by the fluorination of the AE−O bonds. According to the kinetic studies on the formation of monodisperse nanocrystals via the heating-up method, the nucleation process is initiated suddenly while the temperature and supersaturation are being increased as if a switch is turned on.[26a] In our case, as soon as the temperatures are elevated to certain values, the decomposition reaction of these corresponding SSP trifluoroacetate precursors occurs rapidly to give rise to nucleation, as indicated by their steep TG curves, shown in Figure 7. However, as the thermal decomposition reaction of the precursor proceeds further, the supply rate of AEF_2 monomers decreases significantly, and consequently the nucleation process is terminated, and afterward, only the growth process proceeded. In this process, the conditions required for the size-focusing, high supersaturation and no additional nucleation, are both satisfied. As a result, the formation of high-quality AEF_2 nanocrystals can be realized. During this process, due to the strong affinity of the amine groups to the metals,[21] the reaction intermediate partially substituted with OM, that is, $AE(CF_3COO)_{2-x}(OM)_x$ are formed. This finally leads to the formation of AEF_2 nanocrytals with OM molecules capped on their surface, providing their good stability and solubility in nonpolar solvents.

3.2. Luminescence properties of AEF_2 (AE = Ca, Sr, Ba) and CaF_2:Tb^{3+} nanocrystals. AEF_2 (AE = Ca, Sr, Ba) Nanocrystals. Figure 8 shows the excitation and emission spectra of the AEF_2 nanocrystals dispersed in cyclohexane solutions. It is obvious that all three of these fluorides possess similar spectral characteristics, implying the same luminescent mechanism of these materials. The excitation spectra (Figure 8a) of AEF_2 nanocrystals are composed of a broad excitation band between 230 and 290 nm, and their corresponding emission spectra (Figure 8b) show a broad emission band ranging from 275 to 475 nm (CIE color coordinate $x = 0.112$, $y = 0.190$). The presence of a broad band in the excitation and emission spectra indicates that there are a lot of luminescent centers in the obtained AEF_2 nanocrystals. Because bulk AEF_2 crystals do not show luminescence under UV excitation, we can assign this luminescence to the surface defects caused by the high surface-volume ratio of nanocrystals.[12b,30] This viewpoint can be further confirmed by their short lifetime, obtained from the decay curves of AEF_2 nanocrystals in cyclohexane solution, as shown in Figure S3 (Supporting Information). All three luminescence decay curves can be fitted to a single-exponential function as $I = I_0 \exp(-t/\tau)$ (τ is lifetime), from which the lifetimes are determined to be 7.95, 9.66, and 9.65 ns for CaF_2, SrF_2, and BaF_2 nanocrystals, respectively.

CaF_2:Tb^{3+} Nanocrystals. Figure 7 shows the room-temperature excitation and emission spectra of the CaF_2:$0.05Tb^{3+}$ nanocrystal colloidal solution. The excitation spectrum (left part) of CaF_2:$0.05Tb^{3+}$ nanocrystals (monitored by 547 nm of $^5D_4-^7F_5$ of Tb^{3+}) is composed of two relatively strong bands at 230 and 258 nm and some weak bands in the longer-wavelength region (300−500 nm). The former two bands correspond to the spin-allowed ($\Delta S = 0$) and spin-forbidden ($\Delta S = 1$) components of the transitions from the ground state $^7F_6$ of the Tb^{3+} $4f^8$ configuration to the excited state of the $4f^75d$ configuration, respectively.[31] The weak bands in longer-wavelength region (300−500 nm) can be ascribed to the forbidden f−f transitions within the Tb^{3+} configuration. Upon excitation at the $4f^8-4f^75d$ transition at 258 nm, the CaF_2:$0.05Tb^{3+}$ nanocrystals yields characteristic $^5D_4-^7F_J$ ($J = 3, 4, 5, 6$) emissions of Tb^{3+} ions, with a $^5D_4-^7F_5$ emission at 547 nm as the most prominent group (right part). In this situation, the emission is essentially generated from the Tb^{3+} ions, and no emission from surface defects is observed due to their relatively weak intensity with respect to the Tb^{3+} ion emission bands. The digital image of the CaF_2:$0.05Tb^{3+}$ nanocrystal colloidal solution under 254 nm UV lamp irradiation is shown in the inset of Figure 7, demonstrating its high green brightness to the naked eye. The photoluminescence decay curve of CaF_2:

(28) (a) Talapin, D. V.; Rogach, A. L.; Kornowski, A.; Haase, M.; Weller, H. *Nano Lett.* **2001**, *1*, 207. (b) Katari, J. E. B.; Colvin, V. L.; Alivisatos, A. P. *J. Phys. Chem.* **1994**, *98*, 4109. (c) Qu, L.; Peng, Z. A.; Peng, X. *Nano Lett.* **2001**, *1*, 333. (d) Peng, Z. A.; Peng, X. *J. Am. Chem. Soc.* **2001**, *123*, 183. (e) Yu, W. W.; Peng, X. *Angew. Chem., Int. Ed.* **2002**, *41*, 2368. (f) Hines, M. A.; Guyot-Sionnest, P. *J. Phys. Chem. B* **1998**, *102*, 3655. (g) Li, L. S.; Pradhan, N.; Wang, Y.; Peng, X. *Nano Lett.* **2004**, *4*, 2261. (h) Guzelian, A. A.; Banin, U.; Kadavanich, A. V.; Peng, X.; Alivisatos, A. P. *Appl. Phys. Lett.* **1996**, *69*, 1432. (i) Cao, Y. W.; Banin, U. *J. Am. Chem. Soc.* **2000**, *122*, 9692. (j) Battaglia, D.; Peng, X. *Nano Lett.* **2002**, *2*, 1027.

(29) (a) Hambrock, J.; Becker, R.; Birkner, A.; Weiβ, J.; Fischer, R. A. *Chem. Commun.* **2002**, 68. (b) Jana, N. R.; Peng, X. *J. Am. Chem. Soc.* **2003**, *125*, 14280. (c) Murray, C. B.; Sun, S.; Doyle, H.; Betley, T. *Mater. Res. Bull.* **2001**, *26*, 985. (d) Shevchenko, E. V.; Talapin, D. V.; Rogach, A. L.; Kornowski, A.; Haase, M.; Weller, H. *J. Am. Chem. Soc.* **2002**, *124*, 11480.

(30) (a) Lin, C. K.; Luo, Y.; You, H.; Quan, Z.; Zhang, J.; Fang, J.; Lin, J. *Chem. Mater.* **2006**, *18*, 458. (b) Lin, C. K.; Zhang, C. M.; Lin, J. *J. Phys. Chem. C* **2007**, *111*, 3300. (c) Lin, C. K.; Yu, M.; Cheng, Z. Y.; Zhang, C. M.; Meng, Q. G.; Lin, J. *Inorg. Chem.* **2008**, *47*, 49. (d) Zhang, C. M.; Lin, C. K.; Li, C. X.; Quan, Z. W.; Liu, X. M.; Lin, J. *J. Phys. Chem. C* **2008**, *112*, 2183. (e) Green, W. H.; Le, K. P.; Grey, J; Au, T. T; Sailor, M. J. *Science* **1997**, *276*, 1826. (f) Joo, J.; Na, H. B.; Yu, T.; Yu, J. H.; Kim, Y. W.; Wu, F. X.; Zhang, J. Z; Hyeon, T. *J. Am. Chem. Soc.* **2003**, *125*, 11100. (g) Xu, K.; Mao, C. J.; Geng, J.; Zhu, J. J. *Nanotechnology* **2007**, *18*, 315604.

(31) Yu, M.; Lin, J.; Fu, J.; Zhang, H. J.; Han, Y. C. *J. Mater. Chem.* **2003**, *13*, 1413.

$0.05Tb^{3+}$ nanocrystals is shown in Figure S4 (Supporting Information). This curve can be fitted to a single-exponential function as $I = I_0 \exp(-t/\tau)$ (τ is lifetime), from which the lifetimes are determined to be 5.41 ms.

4. Conclusion

In this paper, we present a novel nonhydrolytic route to the synthesis of high-quality AEF_2 (AE = Ca, Sr, Ba) and CaF_2:Tb^{3+} colloidal nanocrystals based on the thermal decomposition of corresponding trifluoroacetate precursors in hot OM, demonstrating the robustness and versatility of the present approach. All of the obtained nanocrystals have uniform morphology and good solubility in cyclohexane solution. Room-temperature luminescent studies have uncovered that the small size effect in terms of the surface-to-volume ratio plays an important role in determining the luminescent behaviors of AEF_2 nanocrystals. After the successful incorporation of Tb^{3+} ions into the CaF_2, bright green luminescence can be observed, which may endow them with potential application as labels for biological molecules.

Acknowledgment. This project is financially supported by the foundation of "Bairen Jihua" of the Chinese Academy of Science, the MOST of China (2003CB314707 and 2007CB935502), and the National Natural Science Foundation of China (NSFC 50572103, 20431030, and 50702057).

Supporting Information Available: XRD patterns (Figure S1) and TG-DTA curves (Figure S2) of p-CaF_2, p-SrF_2, and p-BaF_2, respectively; decay curves (Figure S3) of CaF_2, SrF_2, and BaF_2 nanocrystals dispersed in cyclohexane solutions; decay curve (Figure S4) of CaF_2:$0.05Tb^{3+}$ nanocrystals dispersed in cyclohexane solution. This material is available free of charge via the Internet at http://pubs.acs.org.

IC8014207